CHEMISTRY OF MATERIALS

Article

pubs.acs.org/cm

β-$CuGaO_2$ as a Strong Candidate Material for Efficient Ferroelectric Photovoltaics

Seungwoo Song,[†,‡,⊥] Donghun Kim,[§,⊥] Hyun Myung Jang,[*,†] Byung Chul Yeo,[§] Sang Soo Han,[§] Chang Soo Kim,[‡] and James F. Scott[∥]

[†]Department of Materials Science and Engineering and Division of Advanced Materials Science, Pohang University of Science and Technology (POSTECH), Pohang 37673, Republic of Korea

[‡]Center for New Functional Materials Metrology, Korea Research Institute of Standards and Science (KRISS), Daejeon 34113, Republic of Korea

[§]Computational Science Research Center, Korea Institute of Science and Technology (KIST), Seoul 02792, Republic of Korea

[∥]School of Chemistry and Physics, St. Andrews University, St. Andrews KY16 9AJ, Scotland, United Kingdom

Supporting Information

ABSTRACT: We propose a recently discovered material, namely, β-$CuGaO_2$ [T. Omata et al., *J. Am. Chem. Soc.* **2014**, *136*, 3378] as a strong candidate material for efficient ferroelectric photovoltaics (FPVs). According to first-principles predictions exploiting hybrid density functional, β-$CuGaO_2$ is ferroelectric with a remarkably large remanent polarization of 83.80 $\mu C/cm^2$, even exceeding that of the prototypic FPV material, $BiFeO_3$. Quantitative theoretical analysis further indicates the asymmetric Ga $3d_{z^2}$−O $2p_z$ hybridization as the origin of the $Pna2_1$ ferroelectricity. In addition to the large displacive polarization, unusually small band gap (1.47 eV) and resultantly strong optical absorptions additionally differentiate β-$CuGaO_2$ from conventional ferroelectrics; this material is expected to overcome critical limitations of currently available FPVs.

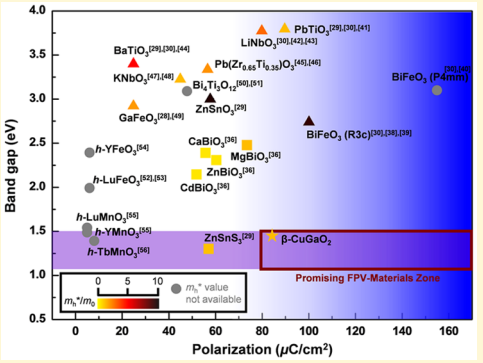

INTRODUCTION

Ferroelectric materials exhibit spontaneous and switchable polarizations due to the breaking of spatial inversion symmetry, which enables these materials to be utilized in extensive technological applications including memory devices,[1−4] microcantilever,[5] and acoustic wave devices.[6,7] Recently, ferroelectric materials have received a renewed attention in light-to-electricity conversion devices owing to their unique coupling of polarizations with optical properties. The ferroelectric photovoltaic (FPV) effect is completely different from the conventional p−n junction PV effect in terms of working principles. In p−n junction diodes, photogenerated electron−hole (e−h) pairs are separated by built-in electric fields forming at an interface, whereas in the case of ferroelectric PVs the e−h pairs are separated by the intrinsic polarizations originating from the lack of centro-symmetry in these materials.[8,9]

Ferroelectric materials have several unique and advantageous features for efficient PV devices. First and foremost, increased output voltage can be obtained in FPVs. In conventional PVs, open circuit voltage (V_{oc}) is well-known to be limited by the band gap energy of a light absorbing material. However, this does not apply to FPVs. Several recent reports have demonstrated that the output V_{oc} of FPVs could be well in excess of the band gap energy of active layer materials with the aid of internal polarizations: V_{oc} values of over 10 V for $BiFeO_3$ (BFO)[10,11] and $Pb(Zr_xTi_{1-x})O_3$ (PZT)[12] were obtained. This implies that ultimate efficiency of FPVs may be able to go even beyond the well-known Schockley−Queisser limit (33.7% for a single junction cell).[13] In addition, strong remanent polarizations in ferroelectric materials provide a driving force for exciton separations throughout the whole absorber layer, rather than just at an interface, which in principle should reduce the charge recombination rates.

Despite the aforementioned features, overall power conversion efficiencies (PCEs) of FPVs have remained very low due to poor photocurrents: short circuit current (J_{sc}) under AM1.5 solar illumination is extremely small, on the order of nA/cm^2.[14] The reported low J_{sc} values are mainly attributed to poor light absorptions. Most ferroelectric materials with sufficiently large polarizations, such as $LiNbO_3$, $BaTiO_3$ (BTO), and PZT, have a very wide band gap energy of >3.0 eV, which places their absorption onset near the ultraviolet (UV).[15−17] BFO is known to have a relatively smaller band gap of 2.7 eV;[18,19] however, this is still far apart from the optimal band gap range (1.1−1.5 eV) for PV applications. In this regard, in order to realize the potential of FPVs, it is highly desirable to search for a novel ferroelectric material with both strong polarization and optimal band gap energy.

Received: July 25, 2017
Revised: August 16, 2017
Published: August 16, 2017

DOI: 10.1021/acs.chemmater.7b03141
Chem. Mater. 2017, 29, 7596−7603

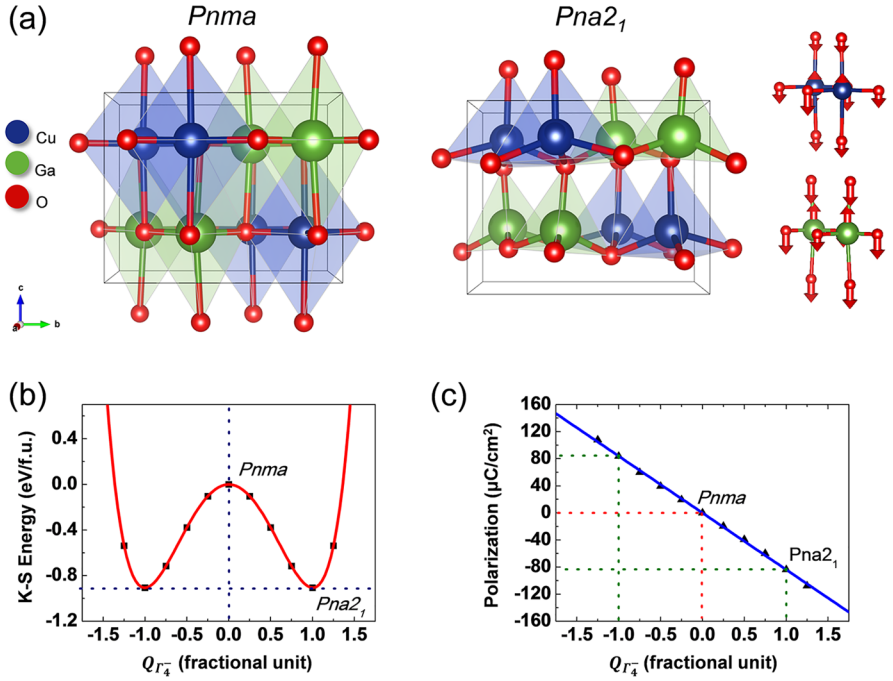

Figure 1. Crystal structures and the associated ferroelectric double-well potential. (a) Optimized crystal structures of the paraelectric *Pnma* (left) and ferroelectric *Pna*2$_1$ (right) phases of $CuGaO_2$. Eigenvectors of the $\mathbf{\Gamma_4^-}$ phonons are denoted by red arrows at the right. (b) Computed K−S energy and (c) polarization values plotted as a function of $\mathbf{Q}_{\Gamma_4^-}$. The reference state where $\mathbf{Q}_{\Gamma_4^-} = 0$ denotes the prototypic *Pnma* structure.

Herein, our focus is a recently discovered material, namely, β-$CuGaO_2$.[20] We employ ab initio density functional theory (DFT) calculation, which has widely been used to estimate the potential of a specific material in PV applications.[21,22] We, for the first time, investigate the promise of β-$CuGaO_2$ in "**ferroelectric**" PVs and prove that this material satisfies the aforementioned particular requirements for efficient FPVs. First, we show that β-$CuGaO_2$ has a sufficiently large ferroelectric polarization of 83.80 $\mu C/cm^2$, which is substantially higher than that of the prototypic FPV material, BFO single-crystal (~60 $\mu C/cm^2$ along ⟨100⟩).[23] Second, β-$CuGaO_2$ exhibits advantageous optical properties. The band gap energy was experimentally measured as 1.47 eV (in the optimal range), and our calculations further predict that it absorbs sunlight much better relative to BFO and silicon. These two features combined together make β-$CuGaO_2$ to overcome major limitations of conventional ferroelectrics, and therefore we propose this material as a strong candidate material for efficient FPVs.

RESULTS AND DISCUSSION

Regarding FPV β-$CuGaO_2$, the precedent point to be clarified is as follows: is it ferroelectric? To answer this critical question, we have calculated the DFT polarization of β-$CuGaO_2$ (space group *Pna*2$_1$) using the Berry-phase formalism within the modern theory of polarization.[24,25] To obtain a correct evaluation of the ferroelectric polarization, a centrosymmetric prototypic phase of $CuGaO_2$ should be first identified. For this, we have exploited the pseudocode of the Bilbao crystallographic server[26] where one can determine the nearest supergroup structure for an input arbitrary structure. In the present case of β-$CuGaO_2$, four centrosymmetric structures were examined: *Pnna*, *Pnma*, *Pbcn*, and *Pccn*. Among these four, the nearest reference structure, in terms of the total displacement of all atoms, turns out to be the *Pnma* phase,

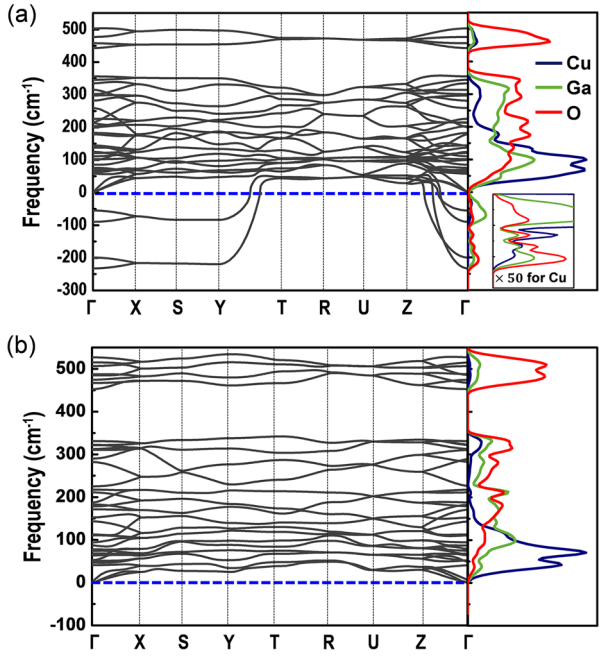

Figure 2. Phononic origin of ferroelectricity. Phonon dispersion curves and corresponding atom-resolved DOSs of $CuGaO_2$ for the (a) paraelectric *Pnma* and (b) ferroelectric *Pna*2$_1$ phases. The inset of (a) is an enlarged representation of the imaginary frequency part.

which has the smallest atomic displacement from the ferroelectric *Pna*2$_1$ phase (see Figure S1 and Table S1 of Supporting Information). The optimized structures of the nonpolar *Pnma* and polar *Pna*2$_1$ phases of $CuGaO_2$ are depicted in Figure 1a. According to group theoretical analysis,[27] there exists only one conceivable transition path that connects the prototypic *Pnma* phase to the ferroelectric *Pna*2$_1$ phase. We have decomposed the atomic displacements related to the

DOI: 10.1021/acs.chemmater.7b03141
Chem. Mater. 2017, 29, 7596−7603

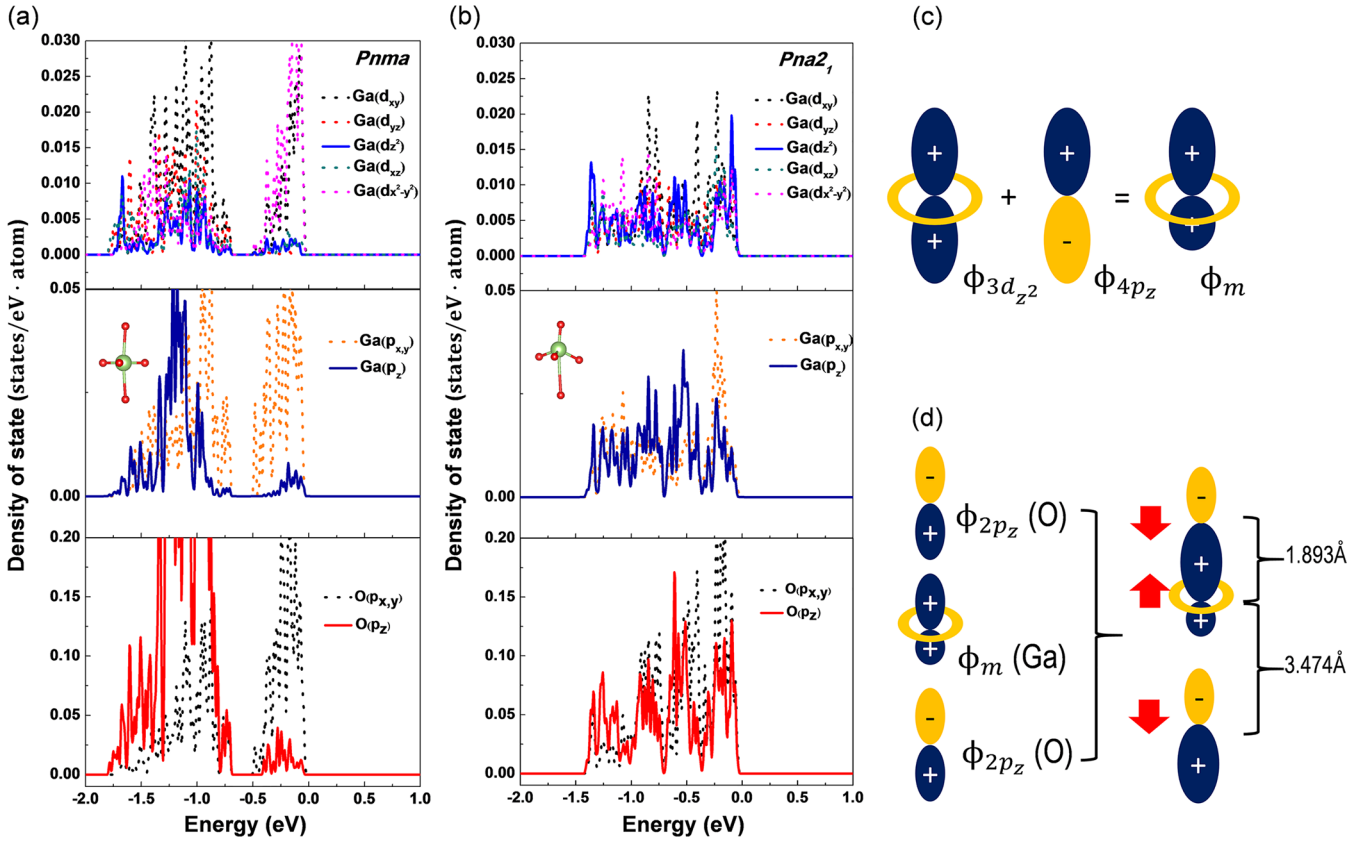

Figure 3. Electronic origin of ferroelectricity. (a, b) Orbital-resolved electronic DOS for Ga 3d, Ga 4p, and O 2p of $CuGaO_2$ for (a) paraelectric *Pnma* structure and (b) ferroelectric *Pna*2$_1$ structure. (c, d) Orbital interaction diagrams that illustrate a sequential bonding mechanism proposed for β-$CuGaO_2$ having the off-centering polarization along the polar *z*-direction: (c) Intra-atomic 3d−4p orbital self-mixing at Ga and (d) asymmetric Ga ϕ_m−O 2p hybridization.

Pnma-to-*Pna*2$_1$ transition into the symmetry-adapted mode of the prototypic phase, and the resulting mode is exclusively given by $\mathbf{\Gamma}_4^-$. Thus, the *Pnma*-to-*Pna*2$_1$ transition should be mediated by freezing in the zone-center $\mathbf{\Gamma}_4^-$ polar phonon.

In Figure 1b,c, the Kohn−Sham (K−S) energy and Berry-phase polarization are plotted as functions of $\mathbf{Q}_{\mathbf{\Gamma}_4^-}$ (i.e., displacement amplitude of the polar $\mathbf{\Gamma}_4^-$ phonon[28]). The computed K−S energy exhibits a double-well-type potential, which indicates the relative stability of the ferroelectric *Pna*2$_1$ phase over the prototypic nonpolar *Pnma* one with the energy difference of 0.9 eV per formula unit (f.u.). The equilibrium ferroelectric polarization of the *Pna*2$_1$ phase is given by the computed polarization values at the two K−S energy minima—namely, ±83.80 μC/cm^2—which corresponds to $\mathbf{Q}_{\mathbf{\Gamma}_4^-}$ of ±1, respectively. At the present stage, an emphasis should be placed on the fact that the polarization strength of β-$CuGaO_2$ is relatively large when compared to well-known ferroelectrics: it is larger than the remanent polarizations of BTO (~25 μC/cm^2), $ZnSnO_3$ (~59 μC/cm^2), and BFO (~60 μC/cm^2) and comparable to those of $LiNbO_3$ (~80 μC/cm^2) and $PbTiO_3$ (~90 μC/cm^2).[29,30]

It is important to note the relatively large barrier energy of 0.9 eV/f.u. In order to show that the ferroelectric switching is feasible in β-$CuGaO_2$, we have searched the barrier energies over a variety of conventional ferroelectrics (28 kinds in total) for comparisons. As a result, many ferroelectrics including well-known $GaFeO_3$ (1.05 eV/f.u.), $BiFeO_3$ (0.43 eV/f.u.), $LiNbO_3$ (0.25 eV/f.u.), and $PbTiO_3$ (0.20 eV/f.u.) are reported to exhibit a ferroelectricity (all cases experimentally measured) despite their large barrier energies. It is true that large coercive electric fields (200−1400 kV/cm) are required for the ferroelectric switching in these materials; however, that does not mean the switching is not possible. Likewise, in the case of our material, β-$CuGaO_2$, we expect a large coercive field (expected >1000 kV/cm) will likely be required in future experiments (see Figure S2 of Supporting Information for a detailed comparison).

The ferroelectric phase transition temperature (T_c) can roughly be estimated from a comparison with the literature. A transition-state theory of rate process predicts that T_c is linearly proportional to the barrier height of the polarization switching. Here, $GaFeO_3$ can serve as a good reference material as it has a similar (slightly larger) barrier height of 1.05 eV with β-$CuGaO_2$. T_c of $GaFeO_3$ was experimentally measured around 1368 K, and thus, β-$CuGaO_2$ with the similar barrier height will likely be stable over the *Pnma* phase up to ~1000 K, although the accurate estimation of T_c requires further follow-up experiments.

Let us now examine the phonon dispersions of paraelectric *Pnma* and ferroelectric *Pna*2$_1$ phases to elucidate the phononic origin of the phase transition. As shown in Figure 2, the ferroelectric *Pna*2$_1$ phase is represented by phonons having real frequencies only. In contrast, the paraelectric *Pnma* phase is characterized by phonon modes with imaginary frequencies (represented as negative values) throughout the Brillouin zone, which indicates that the *Pnma* phase is unstable and needs a symmetry lowering phase transition. Herein, it is important to

DOI: 10.1021/acs.chemmater.7b03141
Chem. Mater. 2017, 29, 7596−7603

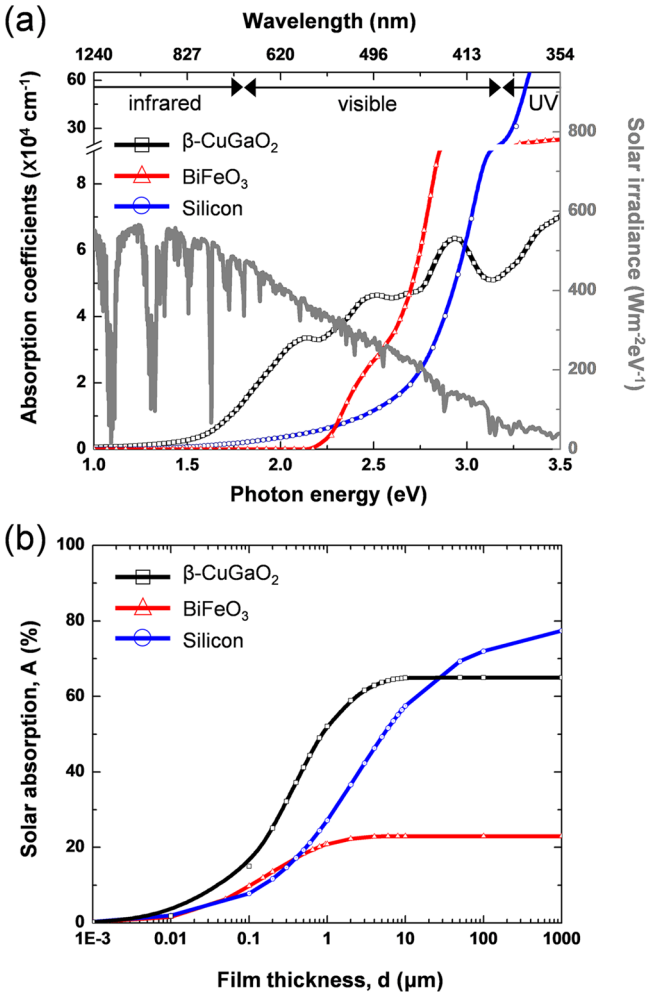

Figure 4. Optical absorption properties of β-$CuGaO_2$, in comparison with BFO and silicon. (a) Absorption coefficients plotted as a function of the photon energy. A gray line represents the AM1.5 solar irradiance. (b) Fractional amount (A) of solar absorptions as a function of the film thickness (d).

note that the instability at the Γ point is quite pronounced, and this is well-known to involve a symmetry lowering with the atomic displacements along the [001] direction. This agrees well with the direction of eigenvectors of the Γ_4^- phonons, as shown in Figure 1a. Among four soft modes (B_{1u}, A_u, B_{2g}, and B_{3g} phonons; see Table S2 of Supporting Information), the condensation of the lowest B_{1u} mode leads to a transition to the ferroelectric $Pna2_1$ phase. Thus, the symmetric B_{1u} transverse-optical (TO) phonon with the strongest instability (i = 232.35 cm^{-1}) at the Γ point is responsible for the $Pnma$-to-$Pna2_1$ transition. Softening of the B_{1u}(TO) phonon is a critical evidence of the displacive-type para-to-ferroelectric phase transition (see Figure S3 of Supporting Information for the B_{1u} eigenvector). More importantly, the atom-resolved phonon DOS further reveals that the phonon softening of the B_{1u}(TO) mode is mainly associated with Ga ions, rather than Cu ions, suggesting that orbital hybridizations between Ga ions and their neighboring O ions would play a significant role in driving the observed ferroelectricity.

Having elucidated the Ga-site-driven ferroelectricity in β-$CuGaO_2$, we have carefully examined electronic DOS for various atomic orbitals involved in the Ga−O bonding interactions. In Figure 3a,b, we compare the orbital-resolved DOSs for Ga 3d, Ga 4p, and O 2p of the paraelectric $Pnma$ phase with those of the ferroelectric $Pna2_1$ phase. The most prominent feature in the computed DOSs is a remarkable enhancement of the $3d_{z^2}$- and $4p_z$-orbital DOSs of Ga (for the energy range between −0.5 and 0 eV below the valence-band top) upon the transition to the ferroelectric $Pna2_1$ state, indicating the intra-atomic Ga $3d_{z^2}$−$4p_z$ orbital self-mixing and the consequent formation of an asymmetric-shaped mixed orbital (ϕ_m), as depicted in Figure 3c. This mechanism of the intra-atomic orbital self-mixing was proposed for a number of oxides such as BFO, $InMnO_3$, and semiconducting ZnO.[31−33] Subsequently, these asymmetric mixed orbitals at Ga (ϕ_m) interact with the two neighboring apical O $2p_z$ orbitals [Figure 3d]. Because of the antisymmetric nature of the $2p_z$ orbital wave function along the z-direction, the Ga ϕ_m−O $2p_z$ orbital overlapping is parity-allowed only for one neighboring Ga−O bond. As a result of this asymmetric overlapping, the Ga atom cannot undergo a simultaneous symmetric bonding interaction with the two apical O atoms along the z-direction. This asymmetric Ga ϕ_m−O $2p_z$ hybridization leads to substantial off-centering displacements along the z-axis [0.79 Å; Figure 3d]. In contrast, the asymmetric 3d−p orbital self-mixing effect is relatively negligible in the case of Cu, due to the fact that Cu 3p contributions are 2 orders of magnitude smaller than Cu 3d ones (see Figure S4 of Supporting Information). Moreover, the ferroelectric off-center displacement along the z-axis is much more pronounced at the Ga-ion site than at the Cu-ion site. Thus, the asymmetric Ga $3d_{z^2}$-O $2p_z$ hybridization (more exactly, Ga ϕ_m−O $2p_z$ hybridization) is mainly responsible for the manifestation of $Pna2_1$ ferroelectricity in β-$CuGaO_2$. This orbital self-mixing mechanism accounts for the appearance of ferroelectricity in an oxide where the 3d orbital of the relevant cation is fully filled (like Ga^{3+} in β-$CuGaO_2$).[32]

Having clarified the existence of the ferroelectricity in β-$CuGaO_2$ with a strong remanent polarization, we assess an optical property of β-$CuGaO_2$ since strong solar absorption is paramount to realizing the potential of FPVs. The band gap energy of β-$CuGaO_2$ is experimentally measured as 1.47 eV,[20] which is in the ideal range (1.1−1.5 eV) for an optimal performance of solar PVs.[13] However, ideal band gap energy does not necessarily guarantee that the material strongly absorbs sunlight. To resolve this critical issue, one must estimate the amount of solar absorptions by calculating the photon-energy-dependent absorption coefficients. For the purpose of comparisons, the solar absorptions of BFO (the best performing material in FPVs to date) and silicon (the most well-known solar absorber) are presented together. For these two materials, absorption coefficient values are reproduced from experimental measurements.[34,35]

A prominent difference between β-$CuGaO_2$ and the other two in Figure 4a is the substantial absorptions of visible and infrared parts of the sunlight. β-$CuGaO_2$ is predicted to absorb more strongly than BFO for the photon energy (E_{photon}) < 2.7 eV and than silicon for E_{photon} < 3.0 eV. For example, at E_{photon} of 2.1 eV, the calculated absorption coefficient (α) of β-$CuGaO_2$ is 3.36 × 10^4 cm^{-1} whereas it is only 4.49 × 10^3 cm^{-1} for silicon and zero for BFO. BFO and silicon become much stronger absorbers than β-$CuGaO_2$ in the UV energy range. However, this UV range constitutes only less than 10% of the total solar spectrum.

With the aforementioned absorption coefficients (α), we can estimate the actual fractional amount (A) of solar absorptions

DOI: 10.1021/acs.chemmater.7b03141
Chem. Mater. 2017, 29, 7596−7603

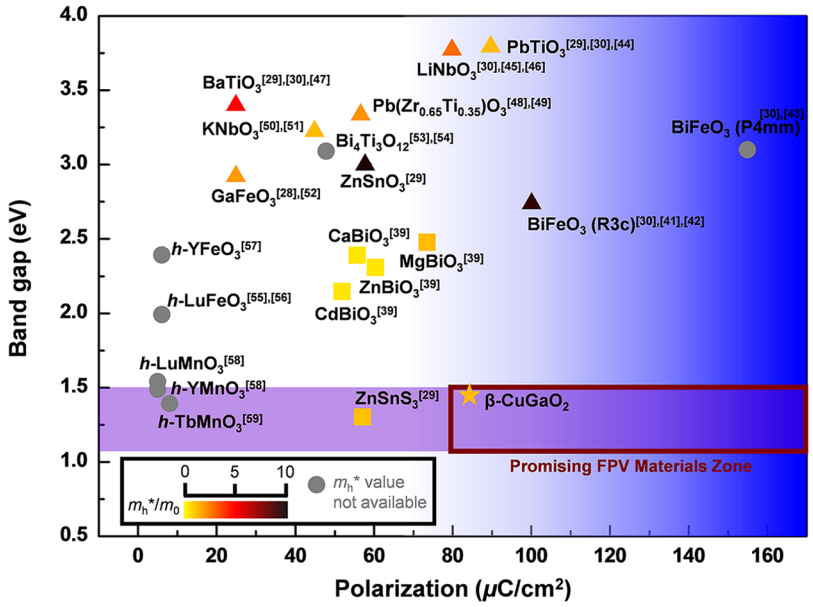

Figure 5. Promise of β-$CuGaO_2$ in FPV estimated by polarization strength, band gap, and hole effective mass. Triangular and circular dots represent conventional ferroelectrics[28−30,38−49] and hexagonal ferrite/magnetite,[50−56] respectively. Squared dots are predicted from theory or computations.[29,36] The "promising FPV material zone" denotes the area with polarization >80 $\mu C/cm^2$ and band gap of 1.1−1.5 eV (a squared boundary marked with a red line) The color code of each dot indicates the hole effective mass (m_h^*/m_0).

as a function of the film thickness (d) using the following equation

$$A\ (\%) = \left(1 - \frac{\int_0^{E_g} S_E\ \mathrm{d}E}{\int_0^{\infty} S_E\ \mathrm{d}E} - \frac{\int_{E_g}^{\infty} \exp(-\alpha d) S_E\ \mathrm{d}E}{\int_0^{\infty} S_E\ \mathrm{d}E}\right) \times 100$$

where S_E is the solar irradiance as a function of the photon energy E [Figure 4b]. The larger absorption coefficients of β-$CuGaO_2$ relative to BFO and silicon (in particular, for the visible and infrared range) result in a greater overall absorption given the same film thickness. In particular, β-$CuGaO_2$ exhibits 2−3 times stronger absorptions than BFO over all thickness ranges. An exception is that silicon absorbs a larger fraction (5−13%) at the saturation level (d > 100 μm), simply because of its lower band gap (1.11 eV). It is important to note that, for β-$CuGaO_2$, the optical absorption nearly saturates at a thickness of 3 μm, whereas silicon does not approach its saturation level until almost 100 μm. This fact suggests that ultrathin films (hundreds of nanometers) of β-$CuGaO_2$ to support reasonable current densities can still absorb effectively enough to be useful. Thus, the use of β-$CuGaO_2$ in FPVs is expected to cause improved currents over most of the ferroelectric materials studied to date.

Finally, we emphasize the promise of β-$CuGaO_2$ in FPV applications by comparing two critical properties—namely, polarization strength and band gap energy—of 17 well-studied ferroelectric materials including β-$CuGaO_2$ (Figure 5). Defining the area with the polarization >80 $\mu C/cm^2$ and band gap of 1.1−1.5 eV as the "promising FPV-material zone", one can readily identify that β-$CuGaO_2$ is the only ferroelectric material falling into this zone, to the best of our research and understanding. Recently, a few materials such as $ZnSnS_3$[29] and $ABiO_3$ (A = Mg, Zn, Cd, Ca)[36] have been theoretically designed to have relatively lower band gap while maintaining decent polarization strength. Unfortunately, however, they have never been experimentally synthesized. Unlike these, the fact that β-$CuGaO_2$ has successfully been synthesized in reality[20,61] can result in timely and direct impacts on the FPV research field.

The search of hole effective masses of these ferroelectric materials offers additional comparisons (Figure 5). It is well-known that, because of weakly hybridized O p-states of the valence band maximum, effective masses of photoexcited holes in various ferroelectric oxides tend to be very large.[37] BFO—currently the best FPV material—also suffers from extremely large hole effective mass (typically 5−20m_0),[30,38,39] which limits the photocurrent enhancements. Hole effective mass of of β-$CuGaO_2$ was previously predicted as 1.7−5.1m_0 (varying with directions) from DFT calculations,[57] which are relatively much smaller than those reported for BFO. From the comparisons of three FPV-relevant properties (polarization, band gap, and hole effective mass), β-$CuGaO_2$ is expected to overcome several critical limitations of conventional FPVs.

CONCLUSION

On the basis of first-principles calculations exploiting accurate hybrid-density-functional, we propose that β-$CuGaO_2$ can be a prime candidate material for efficient FPVs. This material turns out to be ferroelectric with the polarization strength of 83.80 $\mu C/cm^2$. Meticulous analysis of phonon and electronic DOSs was followed, revealing the asymmetric Ga $3d_{z^2}$−O $2p_z$ hybridization as the origin of the $Pna2_1$ ferroelectricity. Unusually small band gap (1.47 eV) of β-$CuGaO_2$ enables the substantial absorption of visible and infrared parts of the sunlight. Compared to 16 other well-known ferroelectrics, β-$CuGaO_2$ is found to be uniquely positioned and can open a new avenue of next-generation FPVs.

COMPUTATIONAL METHODS

All properties investigated in this work (structure, energy, polarization, phonon, density of states (DOSs), and absorption coefficients) were calculated using the plane-wave basis VASP code[58] with an energy cutoff of 500 eV. The projector augmented-wave (PAW) method was

DOI: 10.1021/acs.chemmater.7b03141
Chem. Mater. 2017, 29, 7596−7603

adopted to describe the potential from the ionic core.[59] The hybrid functional of Heyd, Scuseria, and Ernzerhof (HSE06) is used for the exchange-correlation potential.[60] Integration over the Brillouin zone was performed using a Monkhorst−Pack k-piont sampling of 5 × 4 × 5 for structural relaxations and 8 × 6 × 8 for DOSs and absorption coefficients after convergence tests. Geometry is fully relaxed until the force on each atom is less than 0.01 eV Å^{-1}. A total of 32% of the exchange energy is substituted with the Hartree−Fock (HF) exact exchange to make the K−S gap of β-$CuGaO_2$ match with the experimentally known one (1.47 eV). See Figure S5 of Supporting Information for the band gap variation with HF mixing ratio (range between 0 and 35%). Moreover, our computational settings well reproduced experimentally measured crystal structures: the calculated lattice parameters (a = 5.448 Å, b = 6.611 Å, and c = 5.283 Å) are in an excellent agreement with experimental ones,[61] within the deviation of 0.22% for a, 0.01% for b, and 0.16% for c (see Tables S3 and S4 of Supporting Information for detailed comparisons). Overall, the use of hybrid density functional significantly improves both structural parameters and band gap energy of β-$CuGaO_2$, leading to the best accuracy compared to the previous reports.[57,62,63]

Absorption spectra were obtained by computing the complex frequency-dependent dielectric matrix via sums over allowed transitions using the HSE06 eigenvalues in random-phase approximation (RPA) schemes. The absorption coefficients [$\alpha(\omega)$] were calculated from the following equation

$$\alpha(\omega) = \frac{2\omega}{c}\left(\frac{\sqrt{\varepsilon_1^2(\omega) + \varepsilon_2^2(\omega)} - \varepsilon_1(\omega)}{2}\right)^{1/2}$$

where ε_1 and ε_2 are the real and imaginary parts of the dielectric function, respectively, ω is the photon frequency, and c is the speed of light.

■ ASSOCIATED CONTENT

Supporting Information

The Supporting Information is available free of charge on the ACS Publications website at DOI: 10.1021/acs.chemmater.7b03141.

(1) Determination of centrosymmetric supergroup structures, (2) their structural parameters (lattice parameter and fractional coordinates), (3) a comparison of ferroelectric barrier energy for a variety of ferroelectrics (28 kinds in total), (4) optical phonon frequencies of the *Pmna* phase of $CuGaO_2$, (5) B_{1u} eigenvectors, (6) electronic DOS analysis of Cu and its apical O atoms, (7) determination of HF mixing ratio for β-$CuGaO_2$, and (8) optimized lattice parameters and fractional coordinates of each element in β-$CuGaO_2$ (PDF)

■ AUTHOR INFORMATION

Corresponding Author

* E-mail: hmjang@postech.ac.kr.

ORCID

Hyun Myung Jang: 0000-0002-1889-9515

Sang Soo Han: 0000-0002-7925-8105

Author Contributions

⊥(S.S. and D.K.) These authors contributed equally to this work.

Notes

The authors declare no competing financial interest.

■ ACKNOWLEDGMENTS

This work was supported by the National Research Foundation (NRF Grant No. 2016R 1D1A1B 03933253) of Korea and institutional project of KRISS (KRISS-2017-17011067) and KIST (Project No. 2E26940). The authors thank KISTI for providing computational resources (Project No. KSC-2015-C2-033).

■ REFERENCES

(1) Scott, J. F.; Paz de Araujo, C. A. Ferroelectric Memories. *Science* **1989**, *246*, 1400−1405.

(2) Scott, J. F. Applications of Modern Ferroelectrics. *Science* **2007**, *315*, 954−959.

(3) Eerenstein, W.; Mathur, N. D.; Scott, J. F. Multiferroic and Magnetoelectric Materials. *Nature* **2006**, *442*, 759−765.

(4) Jones, R. E., Jr.; Maniar, P. D.; Moazzami, R.; Zurcher, P.; Witowski, J. Z.; Lii, Y. T.; Chu, P.; Gillespie, S. J. Ferroelectric Non-Volatile Memories for Low-Voltage, Low-Power Applications. *Thin Solid Films* **1995**, *270*, 584−588.

(5) Shen, D.; Park, J.-H.; Ajitsaria, J.; Choe, S.-Y.; Wikle, H. C., III; Kim, D.-J. The Design, Fabrication and Evaluation of a MEMS PZT Cantilever with an Integrated Si Proof Mass for Vibration Energy Harvesting. *J. Micromech. Microeng.* **2008**, *18*, 055017.

(6) Sarin Kumar, A. K.; Paruch, P.; Triscone, J.−M.; Daniau, W.; Ballandras, S.; Pellegrino, L.; Marre, D.; Tybell, T. High-Frequency Surface Acoustic Wave Device Based On Thin-Film Piezoelectric Interdigital Transducers. *Appl. Phys. Lett.* **2004**, *85*, 1757−1759.

(7) Sreenivas, K.; Sayer, M.; Baar, D. J.; Nishioka, M. Surface Acoustic Wave Propagation on Lead Zirconate Titanate Thin Films. *Appl. Phys. Lett.* **1988**, *52*, 709−711.

(8) Chynoweth, A. G. Surface Space-Charge Layers in Barium Titanate. *Phys. Rev.* **1956**, *102*, 705−714.

(9) von Baltz, R. Theory of the Anomalous Bulk Photovoltaic Effect in Ferroelectrics. *Phys. Status Solidi B* **1978**, *89*, 419−429.

(10) Yang, S. Y.; Seidel, J.; Byrnes, S. J.; Shafer, P.; Yang, C. H.; Rossell, M. D.; Yu, P.; Chu, Y. H.; Scott, J. F.; Ager, J. W.; et al. Above-Bandgap Voltages from Ferroelectric Photovoltaic Devices. *Nat. Nanotechnol.* **2010**, *5*, 143−147.

(11) Alexe, M.; Hesse, D. Tip-Enhanced Photovoltaic Effects in Bismuth Ferrite. *Nat. Commun.* **2011**, *2*, 256.

(12) Zhang, J.; Su, X.; Shen, M.; Dai, Z.; Zhang, L.; He, X.; Cheng, W.; Cao, M.; Zou, G. Enlarging Photovoltaic Effect: Combination of Classic Photoelectric and Ferroelectric Photovoltaic Effects. *Sci. Rep.* **2013**, *3*, 2109.

(13) Shockley, W.; Queisser, H. J. Detailed Balance Limit of Efficiency of *p-n* Junction Solar Cells. *J. Appl. Phys.* **1961**, *32*, 510−519.

(14) Yuan, Y.; Xiao, Z.; Yang, B.; Huang, J. Arising Applications of Ferroelectric Materials in Photovoltaic Devices. *J. Mater. Chem. A* **2014**, *2*, 6027−6041.

(15) Dhar, A.; Mansingh, A. Optical Properties of Reduced Lithium Niobate Single Crystals. *J. Appl. Phys.* **1990**, *68*, 5804−5809.

(16) Berglund, C. N.; Braun, H. J. Optical Absorption in Single-Domain Ferroelectric Barium Titanate. *Phys. Rev.* **1967**, *164*, 790−799.

(17) Jiang, Y. P.; Tang, X. G.; Liu, Q. X.; Li, Q.; Ding, A. L. Optical Properties of $Pb(Zr_{0.53}Ti_{0.47})O_3$ Thin Films on Pt-Coated Si Substrates Measured by Spectroscopic Ellipsometry in the UV−vis−NIR region. *Mater. Sci. Eng., B* **2007**, *137*, 304−309.

(18) Ji, W.; Yao, K.; Liang, Y. C. Bulk Photovoltaic Effect at Visible Wavelength in Epitaxial Ferroelectric $BiFeO_3$ Thin Films. *Adv. Mater.* **2010**, *22*, 1763−1766.

(19) Basu, S. R.; Martin, L. W.; Chu, Y. H.; Gajek, M.; Ramesh, R.; Rai, R. C.; Xu, X.; Musfeldt, J. L. Photoconductivity in $BiFeO_3$ Thin Films. *Appl. Phys. Lett.* **2008**, *92*, 091905.

(20) Omata, T.; Nagatani, H.; Suzuki, I.; Kita, M.; Yanagi, H.; Ohashi, N. Wurtzite $CuGaO_2$: A New Direct and Narrow Band Gap Oxide Semiconductor Applicable as a Solar Cell Absorber. *J. Am. Chem. Soc.* **2014**, *136*, 3378−3381.

DOI: 10.1021/acs.chemmater.7b03141
Chem. Mater. 2017, 29, 7596−7603

(21) Bernardi, M.; Palummo, M.; Grossman, J. C. Extraordinary Sunlight Absorption and One Nanometer Thick Photovoltaics Using Two-Dimensional Monolayer Materials. *Nano Lett.* **2013**, *13*, 3664−3670.
(22) Raghunathan, R.; Johlin, E.; Grossman, J. C. Grain Boundary Engineering for Improved Thin Silicon Photovoltaics. *Nano Lett.* **2014**, *14*, 4943−4950.
(23) Lebeugle, D.; Colson, D.; Forget, A.; Viret, M. Very Large Spontaneous Electric Polarization in $BiFeO_3$ Single Crystals at Room Temperature and Its Evolution under Cycling Fields. *Appl. Phys. Lett.* **2007**, *91*, 022907.
(24) King-Smith, R. D.; Vanderbilt, D. Theory of Polarization of Crystalline Solids. *Phys. Rev. B: Condens. Matter Mater. Phys.* **1993**, *47*, 1651.
(25) Vanderbilt, D.; King-Smith, R. D. Electric Polarization as a Bulk Quantity and Its Relation to Surface Charge. *Phys. Rev. B: Condens. Matter Mater. Phys.* **1993**, *48*, 4442.
(26) Capillas, C.; Tasci, E. S.; de la Flor, G.; Orobengoa, D.; Perez-Mato, J. M.; Aroyo, M. I. A New Computer Tool at the Bilbao Crystallographic Server to Detect and Characterize Pseudosymmetry. *Z. Kristallogr.* **2011**, *226*, 186−196.
(27) Orobengoa, D.; Capillas, C.; Aroyo, M. I.; Perez-Mato, J. M. AMPLIMODES: Symmetry-Mode Analysis on the Bilbao Crystallographic Server. *J. Appl. Crystallogr.* **2009**, *42*, 820−833.
(28) Song, S.; Lee, J. H.; Jang, H. M. Mode Coupling between Nonpolar and Polar Phonons at the Origin of Improper Ferroelectricity in Hexagonal $LuMnO_3$. *J. Mater. Chem. C* **2014**, *2*, 4126−4132.
(29) Kolb, B.; Kolpak, A. M. First-Principles Design and Analysis of an Efficient, Pb-Free Ferroelectric Photovoltaic Absorber Derived from $ZnSnO_3$. *Chem. Mater.* **2015**, *27*, 5899−5906.
(30) Ederer, C.; Spaldin, N. A. Effect of Epitaxial Strain on the Spontaneous Polarization of Thin Film Ferroelectrics. *Phys. Rev. Lett.* **2005**, *95*, 257601.
(31) Lee, J.; Choi, H. J.; Lee, D.; Kim, M.G.; Bark, C. W.; Ryu, S.; Oak, M.; Jang, H. M. Variations of Ferroelectric Off-Centering Distortion and 3*d*−4*p* Orbital Mixing in La-Doped $BiFeO_3$ Multiferroics. *Phys. Rev. B: Condens. Matter Mater. Phys.* **2010**, *82*, 045113.
(32) Oak, M.; Lee, J.; Jang, H. M.; Goh, J. S.; Choi, H. J.; Scott, J. F. 4*d*−5*p* Orbital Mixing and Asymmetric In 4*d*−O 2*p* Hybridization in $InMnO_3$: A New Bonding Mechanism for Hexagonal Ferroelectricity. *Phys. Rev. Lett.* **2011**, *106*, 047601.
(33) Lee, J. H.; Lee, W.; Lee, S.; Kim, S. M.; Kim, S.; Jang, H. M. Atomic-Scale Origin of Piezoelectricity in Wurtzite ZnO. *Phys. Chem. Chem. Phys.* **2015**, *17*, 7857−7863.
(34) Green, M. A. Self-Consistent Optical Parameters of Intrinsic Silicon at 300K including Temperature Coefficients. *Sol. Energy Mater. Sol. Cells* **2008**, *92*, 1305−1310.
(35) Nechache, R.; Harnagea, C.; Li, S.; Cardenas, L.; Huang, W.; Chakrabartty, J.; Rosei, F. Bandgap Tuning of Multiferroic Oxide Solar Cells. *Nat. Photonics* **2015**, *9*, 61−67.
(36) He, J.; Franchini, C.; Rondinelli, J. M. Ferroelectric Oxides with Strong Visible-Light Absorption from Charge Ordering. *Chem. Mater.* **2017**, *29*, 2445−2451.
(37) Hautier, G.; Miglio, A.; Ceder, G.; Rignanese, G.-M.; Gonze, X. Identification and Design Principles of Low Hole Effective Mass *p*-Type Transparent Conducting Oxides. *Nat. Commun.* **2013**, *4*, 2292.
(38) Yang, C. − H.; Seidel, J.; Kim, S. Y.; Rossen, P. B.; Yu, P.; Gajek, M.; Chu, Y. H.; Martin, L. W.; Holcomb, M. B.; He, Q.; Maksymovych, P.; Balke, N.; Kalinin, S. V.; Baddorf, A. P.; Basu, S. R.; Scullin, M. L.; Ramesh, R. Electric Modulation of Conduction in Multiferroic Ca-Doped $BiFeO_3$ Films. *Nat. Mater.* **2009**, *8*, 485−493.
(39) Ihlefeld, J. F.; Podraza, N. J.; Liu, Z. K.; Rai, R. C.; Xu, X.; Heeg, T.; Chen, Y. B.; Li, J.; Collins, R. W.; Musfeldt, J. L.; et al. Optical Band Gap of $BiFeO_3$ Grown by Molecular-Beam Epitaxy. *Appl. Phys. Lett.* **2008**, *92*, 142908.
(40) Chen, P.; Podraza, N. J.; Xu, X. S.; Melville, A.; Vlahos, E.; Gopalan, V.; Ramesh, R.; Schlom, D. G.; Musfeldt, J. L. Optical Properties of Quasi-Tetragonal $BiFeO_3$ Thin Films. *Appl. Phys. Lett.* **2010**, *96*, 131907.
(41) Scott, J. F.; Schilling, A.; Rowley, S. E.; Gregg, J. M. Some Current Problems in Perovskite Nano-Ferroelectrics and Multiferroics: Kinetically-Limited Systems of Finite Lateral Size. *Sci. Technol. Adv. Mater.* **2015**, *16*, 036001.
(42) Thierfelder, C.; Sanna, S.; Schindlmayr, A.; Schmidt, W. G. Do we know the band gap of lithium niobate? *Phys. Status Solidi C* **2010**, *7*, 362−365.
(43) Mamoun, S.; Merad, A. E.; Guilbert, L. Energy Band Gap and Optical Properties of Lithium Niobate from Ab Initio Calculations. *Comput. Mater. Sci.* **2013**, *79*, 125−131.
(44) Wunderlich, W.; Ohta, H.; Koumoto, K. Enhanced Effective Mass in Doped $SrTiO_3$ and Related Perovskites. *Phys. B* **2009**, *404*, 2202−2212.
(45) Pandey, S. K.; James, A. R.; Raman, R.; Chatterjee, S. N.; Goyal, A.; Prakash, C.; Goel, T. C. Structural, Ferroelectric and Optical Properties of PZT Thin Films. *Phys. B* **2005**, *369*, 135−142.
(46) Zubko, P.; Jung, D. J.; Scott, J. F. Space Charge Effects in Ferroelectric Thin Films. *J. Appl. Phys.* **2006**, *100*, 114113.
(47) Liang, L.; Li, Y. L.; Hu, S. Y.; Chen, L.-Q.; Lu, G.-H. Thermodynamics and Ferroelectric Properties of $KNbO_3$. *J. Appl. Phys.* **2009**, *106*, 104118.
(48) Modak, B.; Ghosh, S. K. Enhanced Photocatalytic Activity on Polarized Ferroelectric $KNbO_3$. *RSC Adv.* **2016**, *6*, 9958−9966.
(49) Neufeld, O.; Toroker, M. C. Play the Heavy: An Effective Mass Study for α-Fe_2O_3 and Corundum Oxides. *J. Chem. Phys.* **2016**, *144*, 164704.
(50) Yao, W. F.; Xu, X. H.; Wang, H.; Zhou, J. T.; Yang, X. N.; Zhang, Y.; Shang, S. X.; Huang, B. B. Photocatalytic Property of Perovskite Bismuth Titanate. *Appl. Catal., B* **2004**, *52*, 109−116.
(51) Irie, H.; Miyayama, M.; Kudo, T. Structure Dependence of Ferroelectric Properties of Bismuth Layer-Structured Ferroelectric Single Crystals. *J. Appl. Phys.* **2001**, *90*, 4089.
(52) Jeong, Y. K.; Lee, J.-H.; Ahn, S.-J.; Jang, H. M. Epitaxially Constrained Hexagonal Ferroelectricity and Canted Triangular Spin Order in $LuFeO_3$ Thin Films. *Chem. Mater.* **2012**, *24*, 2426−2428.
(53) Wang, W.; Wang, H.; Xu, X.; Zhu, L.; He, L.; Wills, E.; Cheng, X.; Keavney, D. J.; Shen, J.; Wu, X.; Xu, X. Crystal Field Splitting and Optical Bandgap of Hexagonal $LuFeO_3$ Films. *Appl. Phys. Lett.* **2012**, *101*, 241907.
(54) Ahn, S.-J.; Lee, J.-H.; Jeong, Y. K.; Na, E.-H.; Koo, Y. M.; Jang, H. M. Artificially Imposed Hexagonal Ferroelectricity in Canted Antiferromagnetic $YFeO_3$ Epitaxial Thin Films. *Mater. Chem. Phys.* **2013**, *138*, 929−936.
(55) Han, H.; Song, S.; Lee, J. H.; Kim, K. J.; Kim, G.-W.; Park, T.; Jang, H. M. Switchable Photovoltaic Effects in Hexagonal Manganite Thin Films having Narrow Optical Bandgaps. *Chem. Mater.* **2015**, *27*, 7425−7432.
(56) Huang, X.; Paudel, T. R.; Dong, S.; Tsymbal, E. Y. Hexagonal Rare-Earth Manganites as Promising Photovoltaics and Light Polarizers. *Phys. Rev. B: Condens. Matter Mater. Phys.* **2015**, *92*, 125201.
(57) Suzuki, I.; Nagatani, H.; Kita, M.; Iguchi, Y.; Sato, C.; Yanagi, H.; Ohashi, N.; Omata, T. First Principles Calculations of Ternary Wurtzite β-$CuGaO_2$. *J. Appl. Phys.* **2016**, *119*, 095701.
(58) Kresse, G.; Furthmuller, J. Efficiency of *Ab-Initio* Total Energy Calculations for Metals and Semiconductors Using a Plane-Wave Basis Set. *Comput. Mater. Sci.* **1996**, *6*, 15−50.
(59) Kresse, G.; Joubert, D. From Ultrasoft Pseudopotentials to the Projector Augmented-Wave Method. *Phys. Rev. B: Condens. Matter Mater. Phys.* **1999**, *59*, 1758.
(60) Heyd, J.; Scuseria, G. E.; Ernzerhof, M. Hybrid Functionals Based On a Screened Coulomb Potential. *J. Chem. Phys.* **2003**, *118*, 8207.
(61) Nagatani, H.; Suzuki, I.; Kita, M.; Tanaka, M.; Katsuya, Y.; Sakata, O.; Miyoshi, S.; Yamaguchi, S.; Omata, T. Structural and Thermal Properties of Ternary Narrow-Gap Oxide Semiconductor; Wurtzite-Derived β-$CuGaO_2$. *Inorg. Chem.* **2015**, *54*, 1698−1704.
(62) Nguyen, M. C.; Zhao, X.; Wang, C. Z.; Ho, K. M. First-Principles Study of Direct and Narrow Band Gap Semiconducting β-$CuGaO_2$. *Mater. Res. Express* **2015**, *2*, 045902.

DOI: 10.1021/acs.chemmater.7b03141
Chem. Mater. 2017, 29, 7596−7603

(63) Suzuki, I.; Nagatani, H.; Kita, M.; Iguchi, Y.; Sato, C.; Yanagi, H.; Ohashi, N.; Omata, T. First-Principles Study of $CuGaO_2$ Polymorphs: Delafossite α-$CuGaO_2$ and Wurtzite β-$CuGaO_2$. *Inorg. Chem.* **2016**, *55*, 7610−7616.

DOI: 10.1021/acs.chemmater.7b03141
Chem. Mater. 2017, 29, 7596−7603